Revista Mexicana de Física **42**, *No. 3 (1996) 414–424*

Thermal resistance of double heterostructure separate confinement GaAs/AlGaAs semiconductor lasers in stripe geometry configuration

E. MARÍN*, I. CAMPS, M. SÁNCHEZ AND P. DÍAZ*
Universidad de La Habana, Facultad de Física
San Lázaro y L, Vedado 10400, Ciudad de La Habana, Cuba
Recibido el 10 de agosto de 1995; aceptado el 9 de enero de 1996

ABSTRACT. The behavior of a laser diode is affected by an increase of temperature within its volume during operation, which is determined by the value of the thermal resistance of the device. In this paper the dependence of this magnitude on different device parameters is calculated for a double heterostructure separate confinement stripe geometry GaAs/AlGaAs lasers. For this purpose the heat conduction equation was solved. The boundary conditions for this problem were derived taken into account different mechanisms of heat extraction from the laser volume and by comparing the contribution of possible heat sources. A detailed study of the influence of these parameters on the thermal resistance value were made. The experimental measured value of the thermal resistance is presented too, for laser diodes of the same structure for which the calculations were made. The structures were grown by means of the low temperature liquid phase epitaxy technique. The low thermal resistance values measured shows the possibilities of this growth method in the performance of AlGaAs lasers with good thermal stability.

RESUMEN. La operación de un láser semiconductor se ve afectada por un incremento de la temperatura en su interior durante su funcionamiento, el cual está determinado por el valor de su resistencia térmica R. En el presente artículo, se calcula la dependencia de esta magnitud de diferentes parámetros del dispositivo en láseres semiconductores de doble heterojuntura y confinamiento separado de portadores y fotones con base en el sistema GaAs/AlGaAs con contacto de franja. Se realiza un estudio detallado de la influencia de estos parámetros sobre el valor de R. Para ello se resolvió la ecuación de la conducción del calor, cuyas condiciones de frontera fueron derivadas considerando los diferentes mecanismos de disipación del calor y comparando la contribución de las diferentes fuentes de calor en el interior de la estructura. Se presentan además mediciones experimentales de R en diodos láser de la misma estructura para la cual se realizaron los cálculos. Las estructuras fueron crecidas mediante epitaxia de la fase líquida a bajas temperaturas. El bajo valor medido para R demuestra las posibilidades de este método de crecimiento para obtener láseres con buena estabilidad térmica.

PACS: 68.55.Df; 73.40.Kp; 85.60.Jb

1. INTRODUCTION

The behavior of a laser diode (LD) is affected by an increase of the temperature within its volume during operation, mainly due to nonradiative recombination processes as well

* Present address: CINVESTAV-IPN, Departamento de Física, Apartado postal 14–740, 07000 México, D.F., México.

as reabsorption of the generated radiation and Joule heating [1]. This temperature increase influences adversely on emission, reliability and the operating characteristics of the laser [2–10]. Therefore, an intense effort has been devoted to LD's thermal properties analyses [1,11–21]. In this work we make a comparison between the different mechanisms of heat extraction from the LD volume and the contribution of all the distributed heat sources within the laser structure are calculated for a typical double heterostructure (DH) separate confinement (SC) stripe geometry GaAs/AlGaAs laser described in Refs. [22,23]. On the basis of these analyses the boundary conditions of the heat conduction equation are derived. This equation was solved assuming steady state conditions in order to evaluate the thermal resistance of the device R and hence the temperature increase within the laser for a given excitation current. The values of R are calculated along the lateral direction of the active region of the laser and its dependence on different parameters is discussed. We also present the experimental measured value of R for LD samples of the same structure sketched in the theoretical model. The laser structures were grown by means of the low temperature (LT) liquid phase epitaxy (LPE) technique. The possibilities of this technique to perform low threshold AlGaAs lasers were demonstrated elsewhere [23], where a threshold current density of 190 A/cm^2 was achieved. The actual state of knowledge in the thermal properties of laser diode devices is reviewed also.

2. HEAT SINKING ANALYSES

The main mechanisms of heat extraction from the laser diode volume are the radiation, the natural convection and the conduction. The rate at which the heat flow generated by a body due to an increase ΔT in the temperature within its volume is evacuated may be expressed as [24]

$$q_{\mathrm{rad}} = \sigma_{\mathrm{B}} \epsilon T_{\mathrm{a}} \Delta T = \alpha_{\mathrm{rad}} \Delta T, \tag{1}$$

$$q_{\mathrm{conv}} = \alpha_{\mathrm{conv}} \Delta T \tag{2}$$

and

$$q_{\mathrm{cond}} = \frac{\sigma}{D} S \Delta T = \alpha_{\mathrm{cond}} \Delta T, \tag{3}$$

for radiation, convection and conduction, respectively. Here S represents the whole surface area of the body, D its thickness, T_{a} is the ambient temperature, σ is the thermal conductivity, σ_{b} is the Stefan-Boltzmann constant, ϵ is the mataerial emissivity and α_{conv} is a constant approximately of the order 10^{-3} W/cm^2 K for most materials [24].

For GaAs, σ is 0.45 W/cm^2 K [25] and ϵ is 0.7 [26]. For a typical LD 100 μm thick, whose width and length are 200 μm and 500 μm, respectively, the proportionality factors are of the following orders: $\alpha_{\mathrm{rad}} = 10^{-4}$ W/cm^2 K, $\alpha_{\mathrm{conv}} = 10^{-3}$ W/cm^2 K and $\alpha_{\mathrm{cond}} = 10^{2}$ W/cm^2 K.

Therefore, the most efficient mechanism of heat extraction is the conduction, which takes place through the bonding wire and the heat sink. The former is negligible because the active region is usually placed very close to the heat sink with higher thermal conductivity, greater surface area and volume than those of the LD. This leads to the fact that

TABLE I. Description of the laser structure studied. The Al composition in the active layer varied from one structure to another, depending on the Al content in the barriers. The heat densities showed are typical calculated values. For this structure the stripe width is 112 μm and the cavity length 800 μm. The typical operation parameters are: Threshold current: 300 mA. Junction Voltage: 1.6 V. Internal Quantum Efficiency of Spontaneous Emission: 0.55. Differential Quantum Efficiency: 0.5. Internal Quantum Efficiency: 1. The lasers were commonly operated in pulsed regime at 300 mA current under 2.4 V forward bias.

Layer	Description	Main heat source	Heat density generated Wm^{-3}	Layer thickness μm	Thermal Conductivity W/cm^3K
AuGe	Ohmic Contact	Joule Heat	4.76×10^5	1.0	150
n-GaAs	Substrate	Joule Heat and reabsorption of radiation	1.85×10^8	100.0	44
n-GaAs	Buffer	Joule Heat and reabsorption of radiation	9.28×10^{12}	2.0	44
n-$Al_{0.7}Ga_{0.3}As$	Cap	Joule Heat	6.82×10^8	1.2	12.9
n-$Al_yGa_{1-y}As$	Barrier	Joule Heat	7.49×10^{10}	0.135	11.87
$Al_xGa_{1-x}As$	Active	Joule Heat, reabsorption of radiation and non radiative recombination	2.05×10^{14}	0.030	17.49
p-$Al_yGa_{1-y}As$	Barrier	Joule Heat	7.49×10^{10}	0.135	11.87
p-$Al_{0.7}Ga_{0.3}As$	Cap	Joule Heat	1.59×10^{11}	0.6	12.9
p-GaAs	Contact	Joule Heat and reabsorption of radiation	9.28×10^{12}	0.3	44
AuZn	Ohmic Contact	Joule Heat	5.0×10^5	1.0	150

almost all the heat is removed directly to the sink. A more detailed comparison between both mechanisms is made in Ref. [27], where we arrived to the conclusion, that nearly the 96% of the total dissipated power is extracted from the LD through the heat sink.

3. HEAT SOURCES

The distribution of heat sources in a semiconductor laser depends upon the conversion efficiency of the energies of the electric and light radiation fields into heat energy and upon the way how these energies are transformed. In Refs. [1, 18] the main heat sources (non-radiative recombination, reabsorbtion of radiation, radiative heat transfer and Joule heating) are described and the expressions that permit the calculation of their contributions are given. In Table I we present the results of our calculations based on this

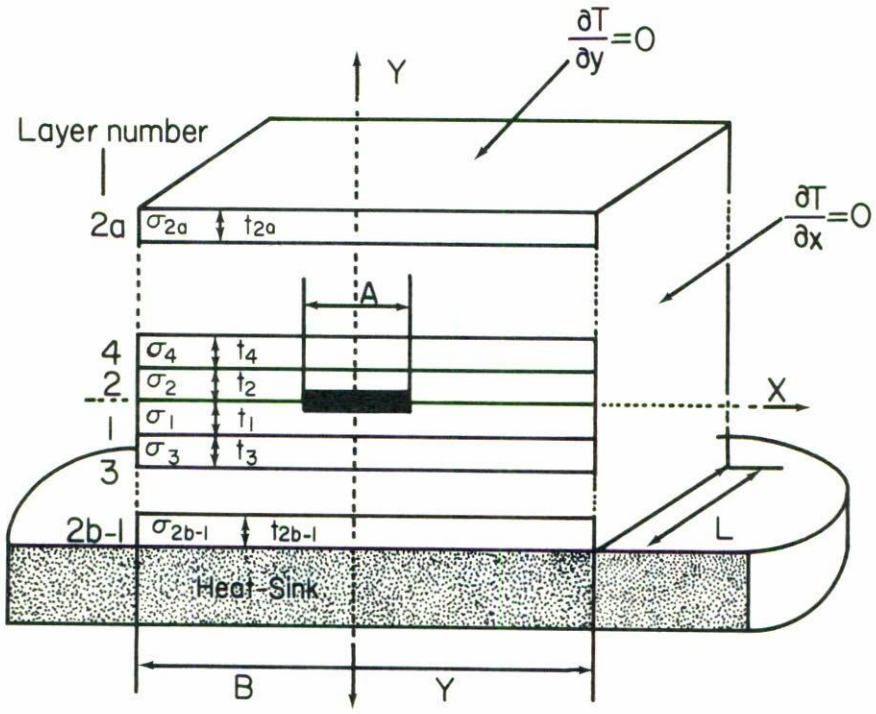

FIGURE 1. Model for calculations.

formalism for the LD structure represented schematically in Fig. 1, where the heat power densities generated in each layer of the structure are listed. Details of calculations are given in Ref. [27]. As we can see, the major contribution is located in the active zone of the device and is mainly due to non-radiative recombination of carriers, reabsorption of the generated radiation and Joule heating. Therefore, this heat source can be considered as a planar stripe embedded at the center of the active region, as was considered by Joyce and Dixon in Ref. [12].

4. BOUNDARY CONDITIONS

Neglecting the mechanisms of radiation, convection and the conduction through the bonding wire, the following conditions are valid (see Fig. 1):

1. No heat flow through the facets:

$$\sigma \left.\frac{\partial T}{\partial x}\right|_{\text{facets}} = 0. \tag{4}$$

2. No heat flow through the upper surface:

$$\sigma \left.\frac{\partial T}{\partial y}\right|_{\text{upper surface}} = 0. \tag{5}$$

3. Due to the high value of the heat sink (HS) thermal conductivity and its dimensions, it may be treated as an infinite medium and its temperature at the external surface becomes the ambient temperature:

$$T_{\mathrm{HS}} = T_{\mathrm{a}}. \tag{6}$$

4. The high carrier concentrations present in the laser structure lead us to consider that the thermal conductivity is temperature independent in the range of interest near T_{a} and then both, the heat flow and the temperature are continuous at the interfaces between the laser layers; therefore

$$\sigma\frac{\partial T}{\partial y} \quad \text{and } T \text{ are continuous at the interfaces.} \tag{7}$$

Nevertheless, in the layers adjacent to the source, the combined flow per unit area coming from both sides is the heat generation rate Q expressed as [12]

$$\sigma_2\frac{\partial T_2}{\partial y}(x,0) - \sigma_1\frac{\partial T_1}{\partial y}(x,0) = \begin{cases} Q, & -\dfrac{A}{2} < x < \dfrac{A}{2} \\ 0, & \left|\dfrac{A}{2}\right| < x < \left|\dfrac{B}{2}\right|. \end{cases} \tag{8}$$

5. MODEL AND SOLUTION

As it has been proposed in Ref. [12] the heat flow can be considered two dimensional and the Laplace equation,

$$\frac{\partial^2 T}{\partial x^2} + \frac{\partial^2 T}{\partial y^2} = 0, \tag{9}$$

with the properly boundary conditions permits the calculation of the temperature $T_i(x,y)$ within the i–th layer with thickness t_i and thermal conductivity σ_i (Fig. 1). This calculation leads to the temperature profile:

$$T_i(x,y) = \beta_{i,0} + \sum_{n=1}^{\infty} \beta_{i,n}(\cosh(k_n y) - \gamma_{i,n}\sinh(k_n y))\cos(k_n y). \tag{10}$$

On the other hand, the thermal resistance is defined as:

$$R_i(x,y) = \frac{T_i(x,y)}{QLA}. \tag{11}$$

The different parameters $\beta_{i,0}$, $\beta_{i,n}$, $\gamma_{i,n}$ and k_n are found from the boundary conditions to be

$$k_n = \frac{2\pi n}{B}, \tag{12}$$

$$\gamma_{2,an} = \tanh(k_n t_{2a}), \tag{13}$$

and

$$\gamma_{2b-l,n} = \coth(k_n t_{2b-1}). \tag{14}$$

The subindices $2a$ and $2b-1$ denotes the outermost structure layers as can be seen from Fig. 1. From the γ values of these layers following an iterative procedure we get:

$$\gamma_{i,n} = \frac{\tanh(k_n t_i) + \frac{\sigma_{i+2}}{\sigma_i}\gamma_{i+2,n}}{1 + \frac{\sigma_{i+2}}{\sigma_i}\tanh(k_n t_i)\gamma_{i+2,n}}. \tag{15}$$

From the innermost coefficient,

$$\beta_{1,n} = \beta_{2,n} = \frac{4Q}{Bk_n^2}\frac{\sin(k_n A/2)}{\sigma_1\gamma_{1,n} + \sigma_2\gamma_{2,n}}, \tag{16}$$

which is obtained from Eq. (8), one arrives to

$$\beta_{i+2,n} = \beta_{i,n}\frac{\coth(k_n t_i) - \gamma_{i,n}}{\coth(k_n t_i) - \gamma_{i+2,n}}. \tag{17}$$

The temperature $T_1(x,0)$ across the active region 1 is

$$T_1(x,0) = \beta_{1,0} + \sum_{n=1}^{\infty}\beta_{i,n}\cos(k_n x), \tag{18}$$

where [27]

$$\beta_{1,0} = \frac{A}{B}Q\left(\frac{t_1}{\sigma_1} + \frac{t_3}{\sigma_3} + \cdots + \frac{t_{2b-1}}{\sigma_{2b-1}}\right). \tag{19}$$

The mean thermal resistance $\bar{R}$ of the device can be calculated by integration of the total resistance in the whole structure volume. For this magnitude we have obtained

$$\bar{R} = \frac{4}{LA^2Y}\sum_{j=2b-1}^{2a}\sum_{n=0}^{\infty}\frac{\beta_{j,n}}{Qk_n^2}\sin(k_n A/2)\sinh(k_n Y/2)Z_{j,n}, \tag{20}$$

where

$$Z_{j,n} = \cosh(k_n Y'/2) \pm \gamma_{j,n}\sinh(k_n Y'/2), \tag{21}$$

$$Y' = t_{2b-1} - t_{2a} \quad \text{and} \quad Y = t_{2b-1} + t_{2a}. \tag{22}$$

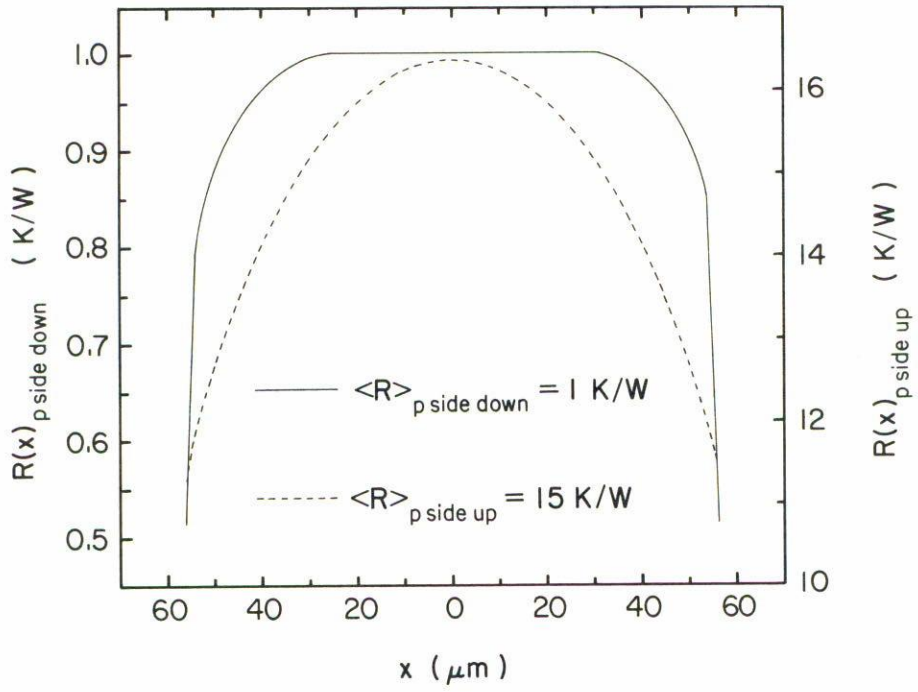

FIGURE 2. Calculated thermal resistance along the lateral direction of the active layer, for two different montage configurations of the device onto the heat-sink. The mean values of the thermal resistance are also shown for both cases.

The sign (+) stands for the montage configuration with the n side of the structure down to the HS (p-side up configuration) and the minus sign (−) for the p-side down configuration. This formula demonstrates that this magnitude has a lower value for a device mounted p-side down onto the HS. Therefore it must be noticed that from the thermal point of view this mounting configuration is the most efficient one.

6. THEORETICAL RESULTS AND DISCUSSION

The obtained expressions allow us to estimate the thermal consequences of changes in the heterostructure parameters. Figure 2 shows the thermal resistance calculated along the active zone of the device whose parameters are listed in Table I. The thermal conductivities of AlGaAs were calculated as indicated in Ref. [25] and the values for the contact metals and metal alloys are found in Ref. [29]. For the p-side down configuration we achieved a mean thermal resistance $\langle R \rangle$ of 1 K/W, while for the p-side up configuration this value is 15 K/W. The value of $\langle R \rangle$ was obtained by integrating Eq. (11); this leads to

$$\langle R \rangle = \frac{1}{A} \int_{-\frac{A}{2}}^{\frac{A}{2}} R_1(x,0)\, dx = \frac{\beta_{1,0}}{QLA} + \frac{2}{QLA^2} \sum_{n=1}^{\infty} \frac{\beta_{1,n}}{k_n} \sin\left(\frac{k_n A}{2}\right). \tag{23}$$

For the operation parameters listed in Table I, the temperature increase in the active zone is 1 K and 13 K, respectively. In the p-up montage configuration the heat flux generated in the active zone must propagate through the substrate, *i.e.*, through a larger distance in order to reach the heat sink. Due to the thermal conductivity and thickness of the substrate the device thermal resistance increases considerably. Thus, the p-down case is desirable if one wants to avoid the device thermal breakdown or a fast degradation when operated at high output power conditions. This, in turn depends on the power supplied to the diode and its conversion efficiency. This is important, since in this welding configuration the thermal resistance of the diode is lowered and hence the raise of the device temperature is less than in the other case. Then, one expect that the device temperature dependent characteristics will behave more stable during the device operation.

Since the diode is welded to the heat sink (in our case Cu), its thermal resistance must be also consider. The presence of several structure layers between the active zone and the HS implies that the heat flux reaches the HS through an area greater than $A \cdot L$ (see Fig. 1). The thermal resistance of a semiinfinite medium is given by [29]

$$\langle R_{\mathrm{HS}} \rangle = \frac{\sinh^{-1}(\xi) + \xi \sinh^{-1}\left(\frac{1}{\xi}\right) - \frac{1}{3}\left(\frac{1}{\xi}(1+\xi^2)^{\frac{3}{2}} - \frac{1}{\xi} - \xi^2\right)}{\pi L \sigma_{\mathrm{HS}}}. \tag{24}$$

where $\xi = L/S_{\mathrm{eff}}$, S_{eff} is the effective area through which the heat reaches the HS and σ_{HS} represents its thermal conductivity.

In order to estimate S_{eff} we have made use of Eq. (11). The calculation was performed by adding to the laser structure a Cu slab of the same surface area of the device and 1 mm thick. This procedure leads to the mean thermal resistance $\langle R \rangle_{\mathrm{HS+laser}}$. The difference $\langle R \rangle_{\mathrm{HS+laser}} - \langle R \rangle$ is the thermal resistance $\Delta\langle R \rangle$ of the added Cu slab. Next, the whole system (laser plus HS) is supposed to be a Cu block with the same heat source as in the laser. The thermal resistance of this Cu block is calculated as a function of the stripe width A. The value of A for which the thermal resistance equals $\Delta\langle R \rangle$ determines the parameter S_{eff} needed to calculate $\langle R \rangle_{\mathrm{HS}}$ by means of Eq. (10).

For the p-down configuration (see Fig. 2) we get for the LD mean thermal resistance $\langle R \rangle$ a value of 1 K/W and for $\langle R \rangle_{\mathrm{HS+laser}}$ 3 K/W, while for the p-up configuration these values are 2 K/W and 15 K/W respectively. From the above results one can see that the consideration of the HS in this analyses is more important for the p-side down configuration.

Now, we will investigate the influence on the thermal resistance of other laser parameters such as: the cavity length, the laser width, the Al content in the active layer and the thickness of the metal bond layer. One can observe from Eq. (23) that the thermal resistance is inversely proportional to the cavity length L. So, one can expect a reduction by a factor of two, if L is twice longer. It must be pointed out, that the optimal condition for the device will not be obtained by simply enlarging the cavity length. Indeed, one have to take into account other laser parameters which depend on L also, for instance and the threshold current density [8] and the conversion efficiency [27].

We have estimated the influence of the diode laser width B on R and it was found that there is not any appreciably change in the value of R. On the other hand, an increase in the stripe width A will reduce considerably the value of R as can be seen in Fig. 3. Here

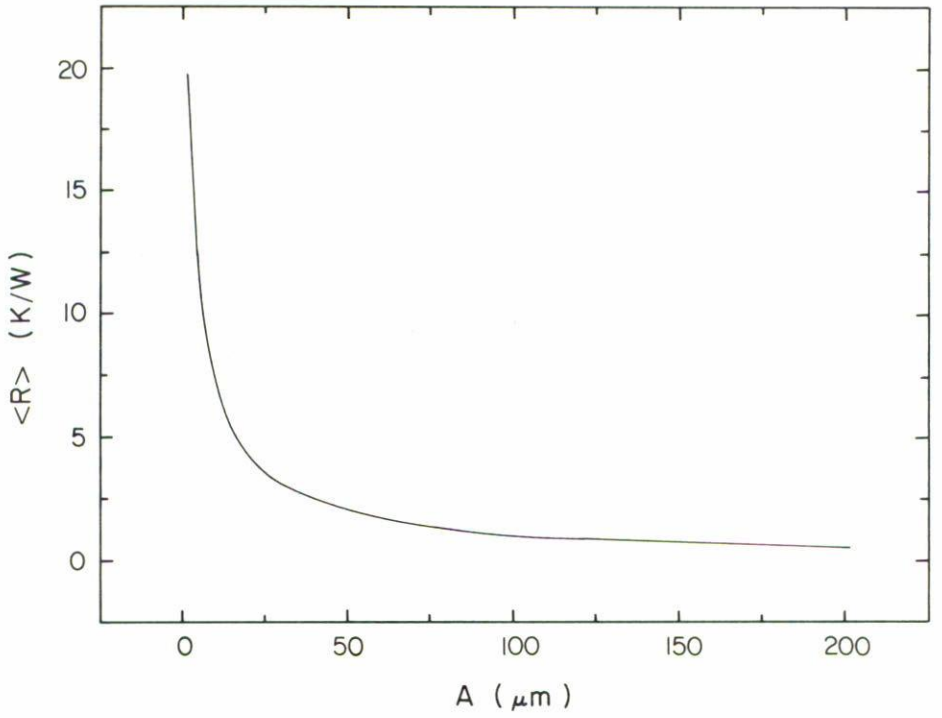

FIGURE 3. Active region mean thermal resistance *vs.* stripe width for the laser structure described in Table I.

again, as was mentioned when we analyzed the R(L) dependence, other laser characteristics dependent on A must be taken into account for device optimization purposes.

The influence on R of the Al content in the active region was also investigated. We did not find in our analyses any appreciable variation of R as a function of the Al content x in the active region. On the other hand, when one considers the metal bond layer (in our case In), it was found that R varies from 1 K/W to 2 K/W as its thickness changes from 1 to 10 μm.

7. EXPERIMENTAL RESULTS

Many methods have been developed to measure the thermal resistance of LD's [1, 15, 29–39]. They are mainly based in measuring any temperature dependent device parameter in continuous (cw) and pulsed operation. The parameters commonly measured are the threshold current density J_{th}, [15, 30], the emission wavelength [15, 29, 31], the junction voltage drop V_0 [15] or the emission power [15, 30]. Because the temperature in the active zone increases by continuous operation of the laser, which not occurs by operation in low duty cycle pulsed regime, it is possible to estimate R measuring the shift of one of the above mentioned parameters when the operation regime is changed from pulsed to cw or from low duty cycle to high duty cycle. In this work R was measured from the shift of

J_{th}. The relationship between the J_{th} values in both regimes is given by [10]

$$J_{\mathrm{th\,cw}} = J_{\mathrm{th\,p}} \exp\left(\frac{\Delta T}{T_0}\right), \tag{25}$$

where ΔT is the temperature increase in the active zone and T_0 is the characteristic temperature of the device. Taken into account the thermal resistance definition, its value can be calculated from

$$R = \frac{T_0 \ln\left(\frac{I_{\mathrm{th\,cw}}}{I_{\mathrm{th\,p}}}\right)}{I_{\mathrm{th\,cw}}\,(V_0 + R_{\mathrm{s}} I_{\mathrm{th\,cw}})}, \tag{26}$$

where R_{s} is the series electrical resistance of the device and I_{th} represents the threshold current. The value of T_0 was determined as described in Refs. [10,27]. Its value was 125 K for one device of the structure described in Table I, for which $L = 264$ μm. The other parameters which enter in Eq. (26) are: $I_{\mathrm{th\,cw}} = 560$ mA, $I_{\mathrm{th\,p}} = 440$ mA, $V_0 = 1.6$ V and $R_{\mathrm{s}} = 2\ \Omega$. The thermal resistance measured value was (20 ± 1) K/W, which agrees quite well with our theoretical predictions in the range of the experimental accuracy. It must be noticed, that the devices for our measurements were LD's chips fixed mechanically onto the copper HS's. The air layer between the HS and the chip can increase considerably R due to the low value of the air thermal conductivity. This fact was not taken into account in calculations, and it could be responsible for differences between the experimental and theoretical values of R.

8. Conclusions

In this paper, we have analyzed the different mechanisms of heat extraction from the volume of DH-SC-AlGaAs stripe geometry lasers. Examining the heat sources distribution within the LD structure, the boundary conditions for the heat conduction equation were justified. This equation was solved in order to obtain the thermal resistance of the device. The achieved expressions allowed us to estimate the thermal consequences of changes in the heterostructure parameters. The thermal resistance of the device was calculated for a given laser structure and its dependence on different parameters was discussed. Our analyses have demonstrated that from the thermal point of view, the p-side down mounting configuration of the device is the most efficient. In this case the influence of the HS thermal resistance must be considered for theoretical and practical purposes. The thermal resistance of the same laser structure used in our model was measured combining the temperature dependence of the threshold current in pulsed and cw operation regimes. Our preliminary experimental results agree quite well with those predicted by our theoretical model. The low thermal resistance value measured here, demonstrates that the LT LPE technique is a suitable one to perform laser structures with high thermal stability. Even though, the applied theoretical model is not the most rigorous, it is helpful for a good understanding of the thermal processes that take place in the LD and it reproduces quite well the experimentally obtained results.

REFERENCES

1. T. Kobayashi, Y. Furukawa, *Jpn. J. App. Phys.* **14** (1975) 1981.
2. M. Ettenberg, C.J. Nuese, H. Kressel, *J. Appl. Phys.* **50** (1979) 2949.
3. N. Chinone, R. Ito, O. Nakada, *J. Appl. Phys.* **47** (1976) 785.
4. S. Ritchie, R.F. Goofrey, B. Wakefield, D.H. Newman, *J. Appl. Phys.* **49** (1978) 3127.
5. W. Nakwaski, *Electron Tech.* **11** (1978) 37.
6. J.Camassel, D. Auvergne, H. Mathieu, *J. Appl. Phys.* **49** (1975) 2683.
7. J.C. Dyment, Y.C. Cheng, A.J. Spring Thorpe, *J. Appl. Phys.* **46** (1975) 1739.
8. M. Sánchez, P. Díaz, G. Torres and J.C. González, *J. Appl. Phys.* **77** (1995) 4259.
9. M. Sánchez, P. Díaz, J.C. González, E. Marín and T. Prutskij, *Rev. Mex. Fís.* **41** (1995) 739.
10. P. Díaz, M. Sánchez, T. Prutskij, E. Marín, J. Hernández and R. Martell, *Proceedings of Workshop on Optoelectronic Materials and their Applications*, La Habana, Cuba (1993), p. 259.
11. P. Garel-Jones. J.C. Dyment, *IEEE J. Quantum Electron.* **QE-11** (1975) 408.
12. W.B. Joyce, R.W. Dixon, *J. Appl. Phys.* **46** (1975) 855.
13. T. Kobayashi, G. Iwane, *Jpn. J. Appl. Phys.* **16** (1977) 1403.
14. D.H. Newman, D.J. Bond, J. Stefan, *Solid State & Electron Device* **2** (1978) 41.
15. E. Duda, J.C. Carballes, J. Apruzzese, *IEEE J. Quantum Electronic* **QE-15** (1979) 812.
16. J. Buus, *IEEE J. Quantum Electronic* **QE-15** (1979) 734.
17. M. Ito, T. Kimura, *IEEE J. Quantum Electronic* **QE-17** (1981) 787.
18. W. Nakwaski, *IEE Proceedings* **131** Pt. I (1984) 94.
19. Y. Lin, Z. Fang, *Electron. Lett.* **27** (1991) 237.
20. G.K. Reeves, S.L. Shi, G.T. Ong, *Electron. Lett.* **28** (1992) 546.
21. G. Chen, C.L. Tien, *J. Appl. Phys.* **74** (1993) 2167.
22. P. Díaz, T.A. Prutskij, M. Sánchez, *Crys. Res. Tech.* **24** (1989) 921.
23. P. Díaz, T.A. Prutskij, F. López, *Crys. Res. Tech,* **25** (1990) 1419.
24. H. Claussnitzer. *Einführung in die Elektrotechnik*, Verlag Technik., Berlin (1965).
25. S. Adachi, *J. Appl. Phys.* **58** (1985) R4.
26. T. Moss, *Semiconductor optoelectronics*, Mir, Moscow (1976) (in russian).
27. I. Camps, Tesis Degree, Faculty of Physics, University of Havana (1995).
28. Y.S. Touloukian (Ed.), *Thermophysical Properties of Matter*, IFI/Plenum, New York-Washington (1973).
29. T. Tsukada and Y. Shima, *IEEE J. Quantum Electron.* **QE-11** (1975) 494.
30. H. Yonezu, T. Yuasa, T. Shinohara, T. Kamejina and I. Sakumada, *Jpn. J. Appl. Phys.* **15** (1976) 2393.
31. T.L. Paoli, *IEEE J. Quantum Electron.* **QE-11** (1975) 498.
32. R.A. Laff, L.D. Comerford, J.D. Crow and M.J. Brady, *Appl. Optics* **17** (1978) 779.
33. J.S. Manning, *J. Appl. Phys.* **52** (1981) 3179.
34. S. Todoroki, M. Sawai and K. Aiki, *J. Appl. Phys.* **58** (1985) 1124.
35. S. Todoroki, *J. Appl. Phys.* **60** (1986) 61.
36. W.C. Tang, H.J. Rosen, P. Vettiger and P.J. Webb, *Appl. Phys. Lett.* **60** (1992) 1043.
37. G. Chen and C.L. Tien, *J. Appl. Phys.* **74** (1993) 2167.
38. F.P. Dabkowski, A.K. Shin, P. Gavrilovic, S. Alie and D.M. Beyea, *Appl. Phys. Lett.* **6** (1994) 13.
39. M. Bertolutti, G. Liakhov, R.L. Voti, R.P. Wang, C. Sibilia and V.P. Yakovlev, *J. Appl. Phys.* **74** (1993) 7054.